Acta Materialia 155 (2018) 12–22

Contents lists available at ScienceDirect

Acta Materialia

journal homepage: www.elsevier.com/locate/actamat

Full length article

Elastic properties of $Al_xCrMnFeCoNi$ ($0 \leq x \leq 5$) high-entropy alloys from *ab initio* theory

Hualei Zhang [a, *], Xun Sun [a, b, **], Song Lu [b], Zhihua Dong [b], Xiangdong Ding [a], Yunzhi Wang [a, c], Levente Vitos [b, d, e]

[a] Center of Microstructure Science, Frontier Institute of Science and Technology, State Key Laboratory for Mechanical Behavior of Materials, Xi'an Jiaotong University, Xi'an, 710049, China
[b] Applied Materials Physics, Department of Materials Science and Engineering, Royal Institute of Technology, Stockholm, SE-100 44, Sweden
[c] Department of Materials Science and Engineering, The Ohio State University, 2041 College Road, Columbus, OH 43210, USA
[d] Division of Materials Theory, Department of Physics and Materials Science, Uppsala University, P.O. Box 516, SE-75120, Uppsala, Sweden
[e] Research Institute for Solid State Physics and Optics, Wigner Research Center for Physics, Budapest, H-1525, P.O. Box 49, Hungary

ARTICLE INFO

Article history:
Received 7 March 2018
Received in revised form
20 May 2018
Accepted 22 May 2018
Available online 24 May 2018

Keywords:
High-entropy alloys
Elastic anisotropy
Brittle/ductile transition
Pugh criterion
First-principles calculation

ABSTRACT

Using *ab initio* calculations, we investigate the elastic properties of paramagnetic $Al_xCrMnFeCoNi$ ($0 \leq x \leq 5$) high-entropy alloys (HEAs) in both body-centered cubic (bcc) and face-centered cubic (fcc) structures. Comparison with available experimental data demonstrates that the employed approach describes accurately the elastic moduli. The predicted lattice constants increase monotonously with Al addition, whereas the elastic parameters exhibit complex composition dependences. The elastic anisotropy is unusually high for both phases. The brittle/ductile transitions formulated in terms of Cauchy pressure and Pugh ratio become consistent only when the strong elastic anisotropy is accounted for. The negative Cauchy pressure of CrMnFeCoNi is due to the relatively low bulk modulus and C_{12} elastic constant, which in turn are consistent with the relatively low cohesive energy. The present findings in combination with the experimental data suggest anomalous metallic character for the HEAs system.

1. Introduction

High-entropy alloys (HEAs) comprising five or more metallic elements have attracted extensive attention from the materials science community since the pioneering works by Yeh et al. [1] and Cantor et al. [2] in 2004. Since then, a new class of HEAs-related materials has been established. The multi-principal element character imposes new challenges as compared to the conventional alloys. The formation of hexagonal close-packed (hcp), face-centered cubic (fcc), and body-centered cubic (bcc) single-phase solid solutions instead of intermetallics or multi-phase systems is usually ascribed to the high mixing entropy and sluggish interdiffusion characteristic of HEAs [1–4]. Nevertheless, so far only a limited number of single-phase solid solutions have been synthesized: fcc CrMnFeCoNi [2,5,6], fcc NiCuRhPdIrPt [7], bcc NbMoTaW and VNbMoTaW [8,9], bcc ZrNbHfTa [10], and hcp FeCoRuRe [11]. Due to the inherent complexity of alloying constituent, HEAs have in general extraordinary damage tolerance and fracture toughness [5,6], excellent and exceptional structural and functional properties [12,13], high thermal stability [14], high hardness [15], combined high strength and ductility [16], corrosion resistance [17], unique magnetic properties [18], with promising potential applications in various technical areas [19–21]. Therefore, the design and development of HEAs with desired properties have become an important subject in materials science and technology.

The five-component CrMnFeCoNi single-phase solid solution is a prototype among large number of HEAs investigated. Several experimental [2,5,6,14,15,22–35] and theoretical studies [36–38] have characterized the structural and mechanical properties of the equiatomic CrMnFeCoNi alloy. It was found that the alloy forms a fcc solid solution at intermediate and high temperatures and possesses good mechanical properties such as high hardness and high bulk modulus [2,5,6]. The alloy was synthesized using mechanical alloying followed by high-pressure sintering [15]. According to the

* Corresponding author.
** Corresponding author. Center of Microstructure Science, Frontier Institute of Science and Technology, State Key Laboratory for Mechanical Behavior of Materials, Xi'an Jiaotong University, Xi'an, 710049, China.
E-mail addresses: hualei@xjtu.edu.cn (H. Zhang), xunsun@kth.se (X. Sun).

https://doi.org/10.1016/j.actamat.2018.05.050
1359-6454/

room-temperature magnetic hysteresis measurements [18], the alloy was found to be paramagnetic (PM), in contrast to MnFeCoNiX (X = Al, Ga, and Sn) alloys, which are ferromagnetic (FM). Recent experiments discovered an irreversible polymorphic transition from fcc to hcp in the alloy under hydrostatic compression at room temperature [22], indicating that the fcc phase is stable at high temperatures while the hcp structure is thermodynamically favorable at low temperatures. The single-crystal elastic constants of the alloy have been determined by first-principles calculations [26] and also measured by a resonance ultrasound spectroscopy at room temperature [27]. The temperature dependence of polycrystalline elastic moduli of alloy have also been established over the temperature range 50–300 K [28] and 200–1270 K [29]. It is generally accepted that all multicomponent solid solutions must have severely distorted lattices. However, the local lattice distortion in equiatomic fcc CrMnFeCoNi HEA measured by neutron scattering is actually moderate [32], suggesting that deviations of local atomic positions from the ideal fcc lattice sites have small impact on the basic physical properties. Indeed, even for refractory HEAs, for which sizable local lattice distortions exist, the influence of lattice distortion on the computed equation of state and elastic properties was recently found to be negligible [39].

To tune the crystal structure and mechanical properties of HEAs, researchers introduced additional alloying elements into the single-phase hosts. A series of investigations on CrMnFeCoNi [38,40] and other HEAs [41–49] found that Al is an effective alloying element. Phase decomposition, such as B2 intermetallic precipitates embedded in a bcc matrix was observed in Al_xCrMnFeCoNi [40] and Al_xCrFeCoNi [44] HEAs at high Al concentrations. The effect of Al on the phase decomposition of CrFeCoNi was studied by first-principles calculations as well [50]. Despite these experimental and theoretical investigations, no first-principles explanation of the observed alloying effects of Al on the elastic properties of CrMnFeCoNi system has been reported so far. The elastic properties are among the most fundamental parameters of solids. It is, however, a highly non-trivial task to determine the elastic parameters of HEAs from first-principles due to inherent complexities associated with multicomponent magnetic systems. In this study, we determine elastic properties of PM Al_xCrMnFeCoNi ($0 \le x \le 5$) HEAs having both bcc and fcc crystal structures using first-principles calculations. The aim is to examine systematically the alloying effect on structure and elastic parameters of the alloy and provide useful inputs to HEAs design.

The rest of paper is divided into three main sections. In Section 2, we give a brief overview of the employed *ab initio* method and present the most important numerical details of the calculations. The calculated single-crystal elastic constants and polycrystalline elastic parameters of the elastic moduli of the Al_xCrMnFeCoNi ($0 \le x \le 5$) HEAs are presented in Section 3. The ductile/brittle behavior is discussed in terms of Cauchy pressure, Pugh ratio, and the newly proposed model by Wang et al. in Section 4.

2. Methodology

The first-principles electronic-structure calculations were performed using the exact muffin-tin orbitals (EMTO) method [51]. We employed the Perdew-Burke-Ernzerhof (PBE) exchange-correlation functional [52] to perform the self-consistent calculations and compute the total energies, i.e. the fully self-consistent PBE scheme was used. We adopted the single-site coherent-potential approximation (CPA) to treat the substitutional and magnetic disorders [53–56]. Using the CPA, one completely ignores the atomic short-range order and local lattice relaxation effects. The first approach is supported by the sluggish diffusion present in HEAs, whereas recent findings confirmed that the absence of severe local lattice distortion in CrMnFeCoNi [32].

We used the scalar-relativistic approximation and soft-core scheme to solve the one-electron Kohn-Sham equations. The Green's function was calculated for 16 complex energy points used to integrate the valence states below the Fermi level. We included *s*, *p*, *d*, and *f* orbitals in the basis set. We used 20 000–25 000 uniformly distributed *k*-points in the irreducible Brillouin zones, which ensures high accuracy for the elastic constants. The electrostatic correction to the CPA was described using the screened impurity model [57] with screening parameter 0.6. The EMTO approach has been successfully applied in the first-principles study of the physical properties of conventional Fe-based alloys [58–65] and multicomponent HEAs [37,39,66–69]. These previous studies indicated that the EMTO-CPA method is a powerful and suitable method in HEAs design.

At room-temperature, the Al_xCrMnFeCoNi alloys have the PM fcc structure at low-Al levels and gradually transform to the PM bcc structure with increasing Al content [38]. However, in low-Al alloys, the theoretical Curie temperature of the thermodynamically unstable bcc phase is above the room-temperature [38]. Since we are primarily interested in phases which can be realized in experiments at room-temperature, here we assume the PM state for all compositions. The PM state was simulated by the disordered local magnetic moment (DLM) model [70]. Within the DLM approach, a PM AlCrMnFeCoNi alloy is described as $Cr^{\uparrow}Cr^{\downarrow}Mn^{\uparrow}Mn^{\downarrow}Fe^{\uparrow}Fe^{\downarrow}Co^{\uparrow}Co^{\downarrow}Ni^{\uparrow}Ni^{\downarrow}$, with equal amount of spin up (↑) and spin down (↓) atoms. Hence, even though the calculations were performed at 0 K, the effect of the loss of magnetization above the Curie temperature was properly captured in the total energy.

There are three independent elastic constants in a cubic lattice: C_{11}, C_{12}, and C_{44}. Dynamical (mechanical) stability requires that $C_{44} > 0$, $C' \equiv (C_{11}\text{-}C_{12})/2 > 0$, and $B > 0$ [71]. In the present study, the cubic elastic constants of the PM Al_xCrMnFeCoNi ($0 \le x \le 5$) alloys were calculated as a function of the chemical composition and crystal structure. At each composition *x*, the theoretical equilibrium volume and bulk modulus were derived from a Morse-type function [72] fitted to the *ab initio* total energies calculated for nine uniformly distributed volumes between 9.1 $Å^3$/atom and 14.4 $Å^3$/atom. This interval includes all equilibrium volumes obtained for $0 \le x \le 5$. There are magnetic transitions within this volume interval (some alloy components develop local magnetic moments with increasing volume) which slightly deteriorates the quality of the numerical fit especially for the bulk modulus. In order to estimate the size of this effect, we show a second set of results for Al-free PM fcc CrMnFeCoNi using a small volume interval (10.4–11.7 $Å^3$/atom) for the Morse fit. However, the alloying induced trends will be considered and discussed using the larger volume interval in order to keep the numerical noises consistent. We neglect the influence of the longitudinal spin fluctuations (LSFs), i.e. we use a static DLM approach. Recently, Dong et al. [73] proposed an accurate and efficient computational scheme for the LSFs in pure Fe as well as in conventional and multicomponent alloys, such as the paramagnetic austenitic steel [74] and CrMnFeCoNi HEA [75]. They found that when LSFs are taken into account, the local magnetic moments vary smoothly with volume. We will return to the effect of LSFs on the elastic constants in Section 3.3.

We used a standard technique [58,59,62] to calculate the single-crystal elastic constants C_{ij}. We obtained the polycrystalline elastic properties from C_{ij} according to arithmetical Hill method [76]. Nevertheless, since the present alloys turned out to be extremely anisotropic, we also discuss results based on the Voigt and Reuss limits as well. The theoretical elastic moduli and single-crystal elastic parameters are used to assess the brittle-ductile behavior using previous empirical correlations.

3. Results

3.1. The Al-free HEA: assessing the accuracy

In Table 1, we list the present theoretical equilibrium lattice parameter a in Å, the single-crystal elastic constants C_{ij} in GPa, the polycrystalline elastic moduli (bulk modulus B, shear modulus G, Young's modulus E) in GPa, the Pugh ratio B/G, the Poisson ratio ν, the Zener anisotropy ratio ($A_Z \equiv C_{44}/C'$), and the Cauchy pressure ($CP \equiv C_{12}-C_{44}$) for PM fcc CrMnFeCoNi. To estimate the effect of volume expansion, in the table we also display the elastic parameters calculated using the room-temperature experimental lattice constant $a_{300K}^{expt.} = 3.594$ Å [40]. The two sets of theoretical results correspond to the two different volume intervals (superscript a: 9.1–14.4 Å^3/atom, b: 10.4–11.7 Å^3/atom). For comparison, several former theoretical [21,26,37,77] and the available experimental data [27,28,78] are quoted.

The present a for PM fcc CrMnFeCoNi, determined from the static DFT calculation adopting the two different volume intervals, are 3.524 and 3.526 Å, respectively, which are very close to each other and close to the former results of 3.528 [77]. Since the elastic parameters are volume-sensitive, there are some small differences between the present two cubic shear moduli C_{44} and C'. But there is 12 GPa difference in the two bulk moduli, 188 versus 176 GPa. Both values are different from the one reported by Tian et al. [77], which can be attributed to the different volume mesh employed when fitting the equations of state. The difference of the bulk modulus causes a difference in C_{11} and C_{12}. Actually, when we adopt the room-temperature experimental volume [40] of CrMnFeCoNi, the bulk modulus obtained for the volume interval 10.4–11.7 Å^3/atom is 147 GPa, which is very close to the experimental data of 144 GPa [27]. Nevertheless, in order to consider the effect of Al on elastic properties of Al$_x$CrMnFeCoNi in a wide Al concentration range, we should adopt the volume interval of 9.1–14.4 Å^3/atom which includes the equilibrium lattice parameters of all Al$_x$CrMnFeCoNi alloys considered here.

The ground state elastic parameters EMTO[a] (0 K, This work) slightly differ from those obtained by Tian et al. [77], which should be ascribed to the numerical parameters adopted in these two works. On the other hand, the large deviations found between the present data and the EMTO results published in Ref. [26] come mainly from the different core-state treatment (soft-core versus frozen-core) and different k-points in the Brillouin zone. Without going into details, we associate the differences between the present EMTO and the former VASP-SQS data [21,26] to the methodological differences (CPA versus supercell, muffin-tin versus full-potential, etc.), to the averaging schemes used for the polycrystalline elastic parameters and to the different magnetic states (PM versus FM) employed in those two studies. Nevertheless, most of the quoted theoretical results predict consistent 0 K data for CrMnFeCoNi.

In addition to the results obtained for the static theoretical volume, in the table we also present EMTO results (denoted by "$a_{300K}^{expt.}$, This work") based on the room temperature experimental volume [40]. The values for C_{44} and C' corresponding to EMTO[a] ($a_{300K}^{expt.}$, This work) are close to the former EMTO results ($a_{300K}^{expt.}$) [37] employing a slightly different experimental volume [29]. The bulk moduli from EMTO[b] ($a_{300K}^{expt.}$, This work) is relatively close to the results by Huang et al. [37], the small differences should be ascribed to the different exchange-correlation approximations employed in those studies. We recall that Huang et al. [37] used the local density appropriation (LDA) for the self-consistent EMTO calculations and the PBE approximation for the total energy (i.e., they adopted a non-self-consistent PBE scheme opposite to the present fully self-consistent PBE scheme).

The single-crystal and polycrystalline elastic constants calculated at 0 K are all higher than the measured data [27,28,78]. That is due to the normal volume effect (negative volume derivatives) associated with the lower (~2%) theoretical static lattice parameter than the measured one [29,40]. On the other hand, the present results obtained for the room temperature volume [40] are much closer to the measured data [27,28,78]. There are two sets of experimental single-crystal elastic constants [27,78], which can be used to define characteristic error bars. Namely, the two data sets reported in Refs. [27,78] differ by 24 GPa, 10 GPa, 37 GPa and 7 GPa for C_{11}, C_{12}, C_{44} and C', respectively. The deviations between the two measurements is partly due to the sample preparation and measuring methods and reflect the intrinsic accuracy of such measurements. Taking the mean experimental values as reference [27,78], for the deviations between our theoretical results EMTO[a] ($a_{300K}^{expt.}$, This work) and the measured data we obtain 14 GPa, 13 GPa, 33 GPa, 1 GPa for C_{11}, C_{12}, C_{44} and C' respectively. These figures are of the same order as the above experimental errors bars indicating that the present theoretical predictions have similar accuracy as the available experimental data.

We observe that the deviations are the largest in the case of C_{44} both between the two sets of experimental data and between the theoretical and experimental values. That is due to the particularly

Table 1
Equilibrium lattice parameter a (Å), single-crystal elastic constants C_{11}, C_{12}, C_{44}, and C'=(C_{11}-C_{12})/2 (GPa), Zener anisotropy ratio ($A_Z = C_{44}/C'$), Cauchy pressure (CP=$C_{12}-C_{44}$) (GPa), polycrystalline elastic moduli B, G, and E (GPa), Poisson ratio ν, and B/G for paramagnetic (PM) fcc CrMnFeCoNi alloy. In addition to 0 K data, we also give our results obtained for the room-temperature experimental lattice parameter [40]. We show the results from two different volume optimization intervals (superscript a: 9.1–14.4 Å^3/atom, b: 10.4–11.7 Å^3/atom). The present results used for the discussion in the coming sections are shown in boldface. Former theoretical results [21,26,37] and available experimental data (in italics) [27,28,78] are listed for comparison. The values marked with * are obtained from standard technique and the Hill averaging method.

	a	Magnetic state	C_{11}	C_{12}	C_{44}	C'	A_Z	CP	B	G	E	ν	B/G
EMTO[a] (0K, This work)	**3.524**	**PM**	**250**	**156**	**180**	**47**	**3.8**	**−24**	**188**	**106**	**267**	**0.263**	**1.78**
EMTO[b] (0 K, This work)	3.526	PM	238	145	179	46	3.8	−33	176	105	262	0.252	1.69
EMTO[a] ($a_{300K}^{expt.}$, This work)	**3.594** [40]	**PM**	**170**	**100**	**143**	**35**	**4.1**	**−43**	**123**	**82**	**201**	**0.228**	**1.51**
EMTO[b] ($a_{300K}^{expt.}$, This work)	3.594 [40]	PM	194	124	143	35	4.1	−19	147	82	207	0.265	1.8
EMTO (0 K) [21] [77]	3.528	PM	245	149	192	48	4.0	−43	181*	111*	276	0.246*	1.63
EMTO (0 K) [26]	3.58	PM	226	160	136	33	4.1	24	184	79	207	0.313	2.33
VASP-SQS (0 K) [26]	3.54	FM	200	97	146	52	2.8	−49	131	97	233	0.204	2.52
VASP-SQS (0 K, energy) [21]	3.536	FM	229	126	146	52*	2.8	−20	160	95	241	0.250	1.68
VASP-SQS (0 K, stress) [21]	3.545	FM	243	134	141	55*	2.6	−7	168	96	241	0.261	1.75
EMTO ($a_{300K}^{expt.}$) [37]	3.6 [29]	PM	187*	117*	138	35	3.9	−21	140	80	201	0.26*	1.75
Expt.(300 K) [27]	-	*PM*	*196*	*118*	*129*	*39*	*3.3*	*−11*	*144*	*80*	*202*	*0.265*	*1.80*
Expt.(300K) [78]	-	-	*172*	*108*	*92*	*32**	*2.8*	*16*	*129**	*61**	*157**	*0.297**	*2.13*
Expt.(300 K) [28]	-	*PM*	-	-	-	-	-	-	*143*	*80*	*202*	*0.265*	*1.79*
Expt.(55 K) [28]	-	*PM*	-	-	-	-	-	-	*145*	*86*	*215*	*0.253*	*1.69*

small C_{44} value reported in Ref. [78], which is far below the other theoretical and experimental values and results in anomalously small shear and Young's moduli compared to the other experimental values [27,28]. In fact the reported C_{44} in Ref. [78] leads to positive Cauchy pressure (*CP*), which is opposite to most of the values listed in Table 1. Exception is the positive *CP* found in Ref. [26] using the EMTO method, which however cannot be taken representative due to the additional (frozen core) approximations employed there. Therefore, we conclude that most of the theoretical and experimental single-crystal elastic constants quoted in Table 1 predict negative Cauchy pressure for CrMnFeCoNi. In other words, according to Pettifor [79], the chemical bonds in the present high-entropy alloy show covalent rather than metallic character despite of the fact that the alloy constituents are considered to have good metallic behavior. We recall that the theoretical Cauchy pressures of the non-magnetic Cr, and ferromagnetic Mn, Co and Ni in the fcc lattice are positive [80], whereas the predicted Cauchy pressure of paramagnetic fcc Fe is negative [81], but the measured value at 1428 K is also positive [82].

From Table 1, by using of data EMTO[a] (0 K, This work) and EMTO[a] ($a^{expt.}_{300K}$, This work), we establish the volume effects on the elastic constants of PM fcc CrMnFeCoNi to be used for later discussions. Comparing the results calculated for lattice parameters 3.594 Å and 3.524 Å, for the mean slopes we obtain $\Delta C_{11}/\Delta a = -1143$ GPa/Å, $\Delta C_{12}/\Delta a = -800$ GPa/Å, $\Delta C_{44}/\Delta a = -529$ GPa/Å and $\Delta C'/\Delta a = -171$ GPa/Å. It is found that all cubic elastic constant follow a normal behavior in terms of volume effect [83], *i.e.* they decrease with expanding volume. Since alloying in general affects the equilibrium volume, one should expect a sizable alloying-driven volume effect in the elastic constants of the present high-entropy alloys.

3.2. Effect of Al doping on the single-crystal elastic constants of CrMnFeCoNi

The single-crystal elastic constants C_{ij} (x) of PM bcc and fcc $Al_xCrMnFeCoNi$ alloys are plotted in Fig. 1 as a function of composition for $0 \le x \le 5$. For each solute concentration x, the present C_{ij} (x) were computed at the corresponding theoretical 0 K (static) equilibrium lattice constant a (x) shown in our former study [38]. It was found that the theoretical equilibrium lattice constant for PM $Al_xCrMnFeCoNi$ alloys increase with increasing Al content, and $\Delta a(x)/\Delta x$ is larger for the fcc structure than that for the bcc one, in line with the available experimental data [40]. Namely, in the low-Al region the theoretical $\Delta a(x)/\Delta x$ for the bcc (fcc) lattice is 0.031 (0.072) Å per Al molar fraction (*i.e.* per x), compared to the mean experimental value of 0.027 (0.10) Å per Al molar fraction. To our knowledge, no experimental or theoretical C_{ij} (x) data are available for the $Al_xCrMnFeCoNi$ system, and hence we continue our discussion by focusing on the theoretical trends in Fig. 1.

As shown in Fig. 1, all individual C_{ij} (x) values predicted for PM bcc and fcc $Al_xCrMnFeCoNi$ possess positive values and fulfill the dynamical stability requirements (*i.e.*, $C_{44} > 0$, $C' > 0$, and $B > 0$) for all x. Theory predicts decreasing $C_{11}(x)$, $C_{12}(x)$ and $C_{44}(x)$ with

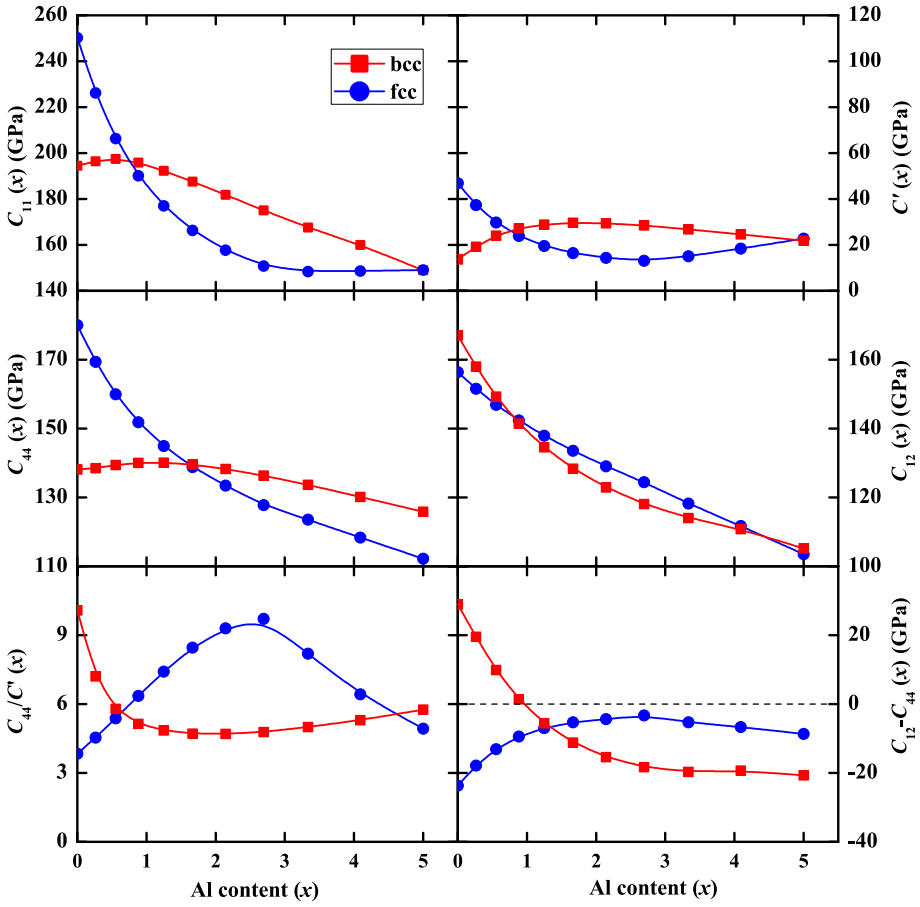

Fig. 1. Theoretical single-crystal elastic constants for paramagnetic bcc and fcc $Al_xCrMnFeCoNi$ ($0 \le x \le 5$) alloys. Zener anisotropy (A_Z) and Cauchy pressure (*CP*) are also presented against Al content. The black dashed line indicates the ductile-brittle limit on the basis of the Cauchy pressure [79]. (For interpretation of the references to colour in this figure legend, the reader is referred to the Web version of this article.)

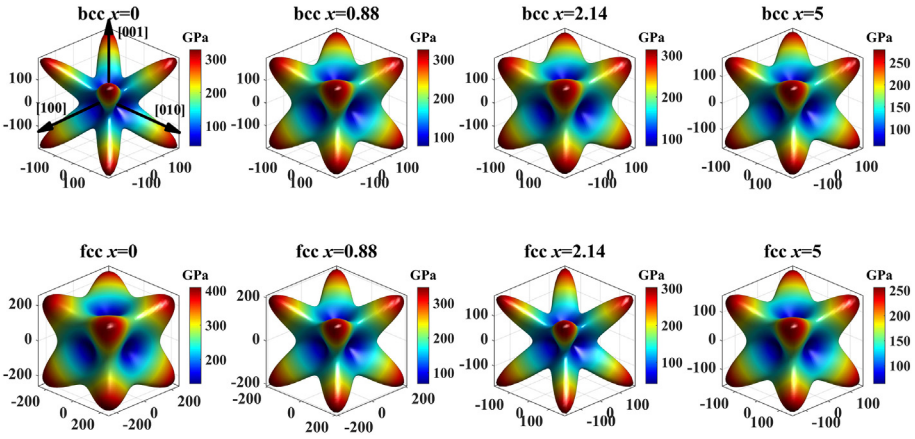

Fig. 2. Three-dimensional surface plots of the single-crystal Young's moduli for paramagnetic bcc (upper panel) and fcc (lower panel) $Al_xCrMnFeCoNi$ alloys as a function Al content ($x = 0$, 0.88, 2.14, and 5). (For interpretation of the references to colour in this figure legend, the reader is referred to the Web version of this article.)

increasing Al content in both fcc and bcc phases. The decreasing $C_{ij}(x)$ implies that Al alloying lowers the elastic stability for both cubic lattices. The two lattices possess similar $C_{12}(x)$ over the entire compositional interval. On the other hand, $C_{11}(x)$ and $C_{44}(x)$ for the fcc phase are significantly larger than those for the bcc phase for $x < 0.76$ and $x < 1.53$, respectively. The different composition dependences obtained for $C_{11}(x)$ and $C_{12}(x)$ for fcc and bcc lattices result in peculiar trends for $C' \equiv (C_{11}\text{-}C_{12})/2$. First, we observe that for all compositions considered here, the calculated $C'(x)$ values are far below the values calculated for the other elastic constants, indicating a rather small energy barrier between the fcc and bcc phases along the usual Bain path. Second, the alloying induced changes in $C'(x)$ are below ~34 GPa, compared to ~102 GPa, ~53 GPa and ~68 GPa, obtained for $C_{11}(x)$, $C_{12}(x)$ and $C_{44}(x)$, respectively. Third, below $x \approx 0.78$, the fcc C' is larger than the bcc one, meaning that the fcc phase is more stable mechanically than the bcc one for low-Al alloys and the bcc phase is mechanically stabilized at high-Al concentrations. Such phenomena agree well with the experimental observations [6,40] and the previous phase stability study [38]. Namely, there is a structural phase transition from fcc to bcc with increasing Al content.

Using the previously established volume effects on the single-crystal elastic constants of fcc CrMnFeCoNi, one can easily separate the volume and chemical effects in the alloying-induced trends in Fig. 1. To this end, we multiply the volume slope $\Delta a(x)/\Delta x$ by the slopes of the fcc elastic constants $\Delta C_{ij}/\Delta a$ to get the slopes $\Delta C_{ij}/\Delta x$ due exclusively to the lattice expansion. The so obtained figures are $\Delta C_{11}/\Delta x = -82.2$, $\Delta C_{12}/\Delta x = -57.9$, $\Delta C_{44}/\Delta x = -38.2$, $\Delta C'/\Delta x = -12.1$ in units of GPa per Al molar fraction. These numbers should be compared to the slopes from Fig. 1 computed at low-Al regime (using two points $x = 0$ and $x = 0.263$), namely −91.2, −18.4, −40.5, −36.6 in GPa per Al molar fraction, respectively. Therefore, in low-Al alloys, the volume effect accounts almost entirely (within ~10%) for the changes calculated for C_{11} and C_{44}. At the same time, the chemical effect in C_{12} turns out to be significant (~40 GPa per Al molar fraction). In other words, C' shows a much stronger decrease with Al doping than the one estimated merely from the volume increase. This phenomenon is clearly due to the strong bcc stabilizing effect of Al when adding to the base high-entropy alloy. We recall that Al decreases the valence electron number and thus brings the alloy towards to stability field of the bcc phase [38].

In Fig. 1 (lower panel), we plot the Zener anisotropy ratio (A_Z) and the Cauchy pressure (CP) for the $Al_xCrMnFeCoNi$ alloys. In this section, we consider the results for the elastic anisotropy, while the trend of the Cauchy pressure will be discussed in details in Section 4. The present HEAs have unusually large elastic anisotropy and show complex concentration dependence with increasing Al content. When compared to the elastic anisotropy of the conventional Fe-based alloys [59], one can see that the present HEAs have significantly more anisotropic lattice than the Fe-based alloys. The bcc A_Z is about twice larger than the fcc one for Al-free alloy, rapidly decreases with x and approaches a minimum at $x \approx 2.14$ with weakly increasing slope at larger Al concentrations. The composition-dependence of the fcc A_Z is different: in low-Al alloys it increases with x, reaches the maximum value (~9.7) at $x \approx 2.69$, above that decreases with x but remains above the Zener anisotropy ratio of fcc CrMnFeCoNi (~4.0) for all x values. Such huge increment of the fcc A_Z is mainly attributed to the substantial drop of the tetragonal elastic moduli $C'(x)$ in the fcc phase with increasing x.

The directional dependence of the Young's modulus associated with the representative surfaces can be used to visualize the elastic anisotropy [84]. The single-crystal Young's modulus E [hkl] for direction [hkl] can be expressed as [85].

$$1/E[hkl] = S_{11} - 2(S_{11} - S_{12} - S_{44}/2)\left(n_1^2n_2^2 + n_2^2n_3^2 + n_1^2n_3^2\right)$$

where $S_{11}=(C_{11}+C_{12})/[(C_{11}\text{-}C_{12})(C_{11}+2C_{12})]$, $S_{12} = \text{-}C_{12}/[(C_{11}\text{-}C_{12})(C_{11}+2C_{12})]$ and $S_{44} = 1/C_{44}$ are the elements of the elastic compliance matrix (inverse of the elastic stiffness matrix). $n_1 = h/m$, $n_2 = k/m$, $n_3 = l/m$ are the direction cosines corresponding to the direction [hkl] and $m = \sqrt{h^2 + l^2 + k^2}$.

In Fig. 2, we plot the three-dimensional single-crystal Young's moduli of $Al_xCrMnFeCoNi$ system for a few compositions. One can see that the anisotropy in the bcc phase first decreases with increasing Al content and reaches a minimum value near $x = 2.14$, and then slightly increases with further increasing the Al concentration. The anisotropy of the fcc structure first increases (up to $x = 2.14$) and then weakly decreases with further Al addition. It is worth noting that for both fcc or bcc structures, the largest (smallest) value of E is along the <111> (<100>) direction.

3.3. Polycrystalline elastic parameters

In Fig. 3, we presented the theoretical polycrystalline elastic properties (bulk modulus B, shear modulus G, Young's modulus E, Pugh ratio B/G, Poisson ratio ν, and elastic Debye temperature Θ) for the PM bcc and fcc $Al_xCrMnFeCoNi$ ($0 \le x \le 5$) alloys. The present

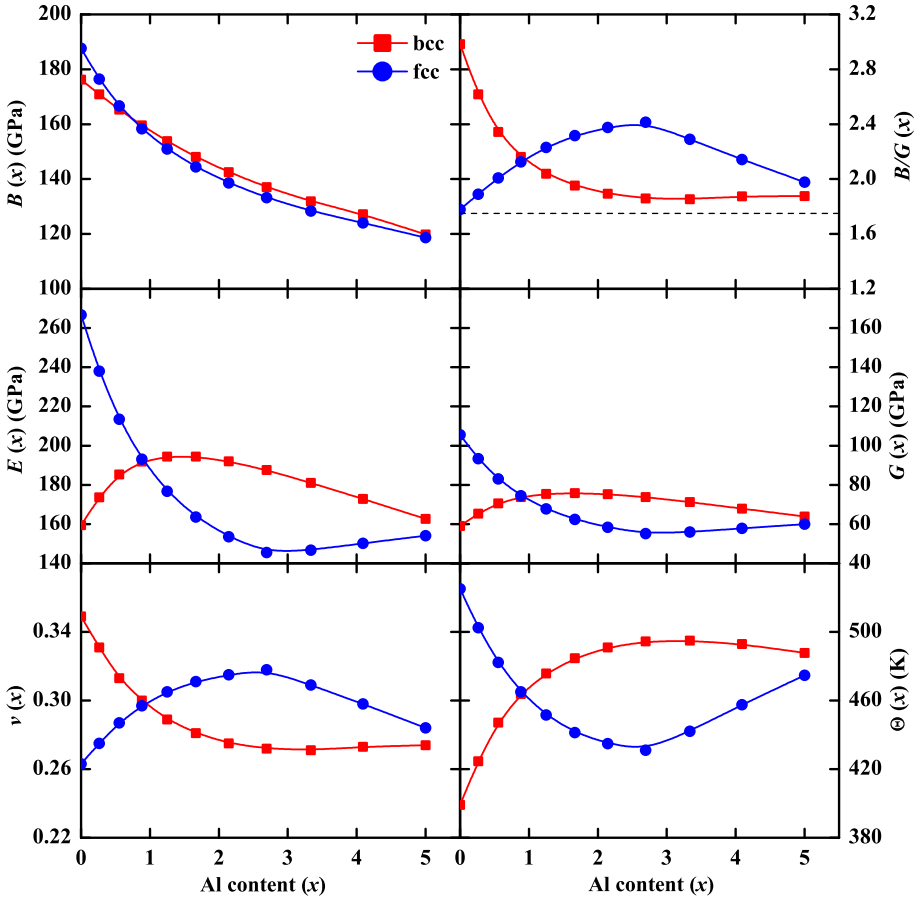

Fig. 3. Theoretical polycrystalline elastic parameters for paramagnetic bcc and fcc $Al_xCrMnFeCoNi$ ($0 \le x \le 5$) alloys. The black dashed line indicates the ductile-brittle limit by Pugh [91]. (For interpretation of the references to colour in this figure legend, the reader is referred to the Web version of this article.)

polycrystalline elastic parameters are derived from the 0 K single-crystal elastic constants shown in Section 3.2 according to the Hill average method. In lack of experimental polycrystalline elastic moduli for $Al_xCrMnFeCoNi$ alloys, here we focus on the theoretical trends. Theory predicts negative slopes for $B(x)$ in both bcc and fcc phases within the entire composition range, reflecting the increased equilibrium volume shown in our former study [38]. On the other hand, $E(x)$ and $G(x)$ display complex composition dependence, similar to the situation found for the single-crystal elastic constants shown in Fig. 1. For all compositions, the Pugh ratio B/G remains above the empirical ductility limit, suggesting that the present systems are ductile. We will return to this observation in the following section.

The largest differences between the two Debye temperatures are obtained for the low-Al and intermediate-Al containing alloys, indicating that for these systems phonons could substantially influence the phase stability. Using the high-temperature phonon free energy expansion [86], at 300 K the phonon effect is estimated to decrease the thermodynamic stability of the fcc phase by more than 0.5 mRy in alloys with x below ~0.65 and increase it by more than 0.5 mRy in alloys with x between ~3 and ~5, for which the two Debye temperatures differ by ~10%. Compared to the structural energy differences reported in Ref. [38], the above phonon free energy differences are small but not negligible especially when considering even higher temperatures. For a quantitative phonon free energy calculation, however, one should compute the phonon spectra for both lattices as a function of chemical composition. Today this task is beyond the reach of *ab initio* alloy tools. We should acknowledge the recent efforts along this line. Wang et al. [87] adopted the quasi-harmonic phonon approximation [88] to compute the vibrational free energy of refractory HEAs. Körmann et al. [89] calculated the phonon spectra of refractory HEAs using the *ab initio* approach. Ikeda et al. [90] developed an efficient method to account simultaneously for the thermal magnetic fluctuations and chemical disorder. So far, the method was demonstrated on a couple of binary magnetic alloys.

Before turning to the discussion, we review the main approximations adopted in the present calculations. First, we estimate the effect of LSFs. Dong et al. [74] found that taking into account the LSFs increases A_Z of PM fcc Fe15Cr15Ni by ~ 12%. Performing similar calculations for PM fcc CrMnFeCoNi (not shown), we obtain that when the LSFs at room temperature are considered, C' decreases by ~3 GPa and C_{44} remains almost unchanged, compared to the static DLM values. These effects result in ~10% increase of A_Z, which may be considered the error due to the neglect of LSFs. Second, we observe that the theoretical results EMTO[b] ($a_{300K}^{expt.}$, This work) in Table 1 are close to the experimental values [27], meaning that the explicit lattice excitations should have small effect on the elastic constants at room temperature. Third, according to Feng's work [92], the chemical short-range order has a negligible effect (less than 2%) on the Zener anisotropy of $FeCoNi(AlSi)_x$ HEAs. Because of the above findings, we expect that the present elastic constants and elastic anisotropy are robust even though the magnetic and lattice excitations and the chemical short-range order have been omitted.

4. Discussion

Based on the calculated elastic parameters, we can make some attempts to predication the mechanical properties of the $Al_xCrMnFeCoNi$ alloys. Negative Cauchy pressure (*CP*) describes increased degree of covalent bonding character for crystals, while positive Cauchy pressure stands for more metallic character [79]. These two binding characters are often associated with ductile and brittle behavior, respectively. In Fig. 1 (lower panel), the theoretical *CP* value for the Al-free alloy is 29 GPa (−24 GPa) in the bcc (fcc) phase, implying that Al-free alloy is ductile (brittle) in the bcc (fcc) phase. But according to the experimental results [6], the Al-free CrMnFeCoNi alloy is stable in the fcc structure and is ductile. Therefore estimating the ductility based on the Cauchy pressure seems to lead to a contradiction between theory and observation for the present HEAs. One might attribute this contradiction to the complex chemical interactions in the HEAs, which apparently does not follow the common behavior observed for metals and traditional alloys.

Here we use the calculated Cauchy pressures to analyze the ductile/brittle behavior as a function of composition. When adding a small amount of Al (x below ~1) to CrMnFeCoNi, the Cauchy pressure of the bcc phase decreases and that of fcc increases, so that the fcc phase becomes more ductile and the bcc phase more brittle. For x above ~1, the Cauchy pressures of the bcc phase drops below that of the fcc phase and remains the lowest for high-Al alloys. We can also compare the present theoretical Cauchy pressure values obtained for $Al_xCrMnFeCoNi$ to those calculated for $Al_xCrFeCoNi$ [67]. It is found that at all Al levels, the equiatomic Mn addition decreases the Cauchy pressure and thus makes the system relatively more brittle.

Pugh suggested that the *B*/*G* ratio measures the ductility and brittleness of solids [91]. The ductile/brittle limit was placed at $Pugh_0 = 1.75$, which is a robust empirical boundary established based on a large number of solids [58,93]. In general, ductile (brittle) alloys are characterized by *B*/*G* ratios larger (smaller) than the above empirical limit $Pugh_0$. For isotropic polycrystalline materials, the Poisson ratio v is connected to *B*/*G* as $v = (3B/G\text{-}2)/(6B/G+2)$. Thus the $B/G = Pugh_0$ boundary corresponding to $v_0 = 0.26$. Accordingly, the above ductility criterion of alloys draw from the Pugh ratio implies $v > 0.26$ based on the Poisson ratio. Indeed, for the present alloys, the Pugh and Poisson ratios obey similar nonlinear concentration dependences as shown in Fig. 3. Based on the Pugh and Poisson standards, we find that the *B*/*G* and v of the $Al_xCrMnFeCoNi$ alloys in bcc phase first strongly decrease and then keeps almost unchanged with increasing Al content, while the *B*/*G* and v in the fcc phase first increase and then weakly decrease with increase x. We note that in terms of the Pugh ratio, the bcc phase is much more ductile than the fcc one at low-Al region. However, the fcc alloy becomes more ductile than the bcc one at $x > 1.0$. Similarly to the case of the Cauchy pressure, the Pugh ratio of $Al_xCrMnFeCoNi$ is also lower than that of $Al_xCrFeCoNi$ [67], indicating that the Mn addition makes the system more brittle.

We observe that the Pugh ratios have the same trends as the Cauchy pressures (Figs. 1 and 3). Nevertheless, the associated critical values, *i.e.*, $CP_0 = 0$ and $Pugh_0 = 1.75$, are totally inconsistent for the present alloys. Similar observation was made on other HEAs as well [67]. We argue that the reason behind the inconsistency is the unusually large elastic anisotropy which gives rise to large uncertainties in the polycrystalline elastic moduli and thus in the Pugh ratio. We note that the bulk modulus is well defined for a polycrystalline material consisting of grains with cubic lattice and thus the averaging method affects the Pugh ratio only through the shear modulus.

The polycrystalline shear modulus *G* is obtained from the single-crystal data according to the Voigt-Reuss-Hill averaging method [56]. The G_V and G_R draw from the Voigt and Reuss averaging methods have the following expressions

$$G_V = \frac{C_{11} - C_{12} + 3C_{44}}{5} \text{ and } G_R = \frac{5(C_{11} - C_{12})C_{44}}{5C_{44} + 3(C_{11} - C_{12})}$$

The Hill value usually represents the arithmetical average of the above bounds. We point out that for elastically isotropic materials ($A_Z = 1$) we have $G_V = G_R$ and thus the uncertainty in the shear modulus disappears. However, when A_Z is large, *B*/*G* varies very differently in the above averaging methods [94]. Our calculated anisotropy A_Z for PM bcc (fcc) $Al_xCrMnFeCoNi$ alloys are 5–10 (4–9), respectively. Hence, A_Z of the present HEAs is far greater than that of the most traditional alloys (*e.g.*, $A_Z = 1.3$–1.6 for FeMn and $A_Z = 1.3$–1.8 for FeNi) [94] and thus should be accounted for them comparing the Pugh and Cauchy criteria.

Below we discuss the relation between Pugh ratio *B*/*G* and Cauchy pressure *CP* considering the elastic anisotropy. First, we take the relation based on the Voigt averaging method. Using the definition of the Cauchy pressure, we get $CP{=}B - 5/3G_V$. We note that this expression is very close to $CP/B = -1.620\text{G/B}{+}0.995$ obtained by fitting the experimental data by Wang et al. [95]. Using the above theoretical expression, the criterion for ductility based on the Cauchy pressure $CP > 0$ in terms of the Pugh ratio based on the Voigt method reads $Pugh_0^V \equiv B/G_V > 5/3 \approx 1.67$. It is important that the connection between the Cauchy pressure and the Pugh ratio obtained using the Voigt method does not depend on the elastic anisotropy.

When we adopt the Reuss or Hill averaging method, the relation between Cauchy pressure and Pugh ratio cannot be expressed as simple as in the case of Voigt method. Because of that, next we discuss the critical Pugh ratio ($Pugh_0$) corresponding to $CP_0 = 0$ (*i.e.* in the following expressions we assume vanishing Cauchy pressure). We find that $Pugh_0$ can be expressed as a function of Zener anisotropy A_Z as

$$Pugh_0^R(A_Z) = \frac{1}{15}\left(\frac{6}{A_Z} + 13 + 6A_Z\right),$$

in the Reuss case and

$$Pugh_0^H(A_Z) = \frac{10}{3}\frac{1}{\frac{25}{\frac{6}{A_Z}+13+6A_Z}+1},$$

in the Hill case.

In Fig. 4, we show the Pugh criteria based on the Reuss, Hill and for reference also on the Voigt methods. We find that $Pugh_0$ in the three averaging methods are all 1.67 when $A_Z = 1$, whereas $Pugh_0^R$ increases rapidly when A_Z deviates from 1. On the other hand, $Pugh_0^H$ increased slower than $Pugh_0^R$ because of the contribution coming from the Voigt method. For low anisotropies ($A_Z = 0.5$–2), we have $Pugh_0^V = 1.67$, $Pugh_0^R = 1.67 \sim 1.87$, and $Pugh_0^H = 1.67 \sim 1.76$. Hence, since A_Z lies within the range of 0.5–2 for most metals and alloys [96,97], the semiempirical ductility/brittleness boundary of $B/G = 1.75$ seems to be appropriate. This explains why the Cauchy pressure and Pugh ratio criterion provide similar conclusions [98] in most cases. However, the PM $Al_xCrMnFeCoNi$ alloys has an ultra-high Zener anisotropy A_Z both in bcc and fcc phase. Then the *B*/*G* criterion changes as a function of the A_Z if we consider $CP = 0$ as the measure of the bonding character.

In Fig. 4, we plot the Pugh ratios of the present PM fcc and bcc $Al_xCrMnFeCoNi$ alloys as a function of the elastic anisotropy. It is found that most of the Pugh ratios are indeed lower than the

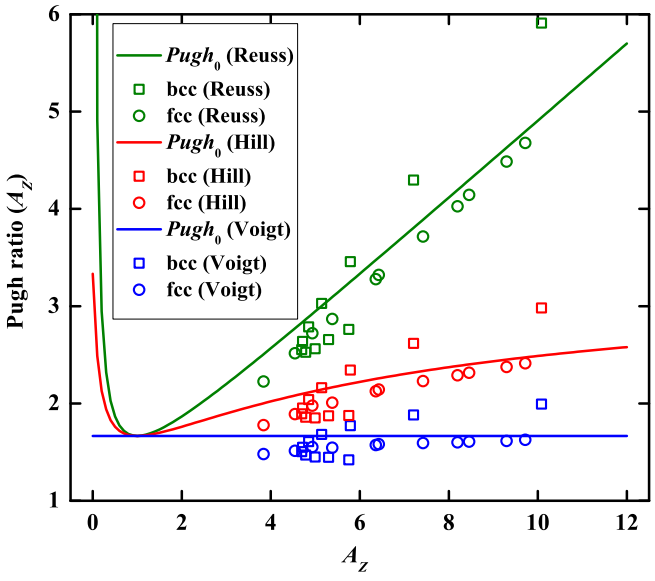

Fig. 4. Pugh criterion ($Pugh_0$) as a function of Zener anisotropy A_Z in the Voigt, Reuss and Hill averaging methods. We also display the Pugh ratio of paramagnetic bcc and fcc $Al_xCrMnFeCoNi$ corresponding to different Zener anisotropy A_Z. (For interpretation of the references to colour in this figure legend, the reader is referred to the Web version of this article.)

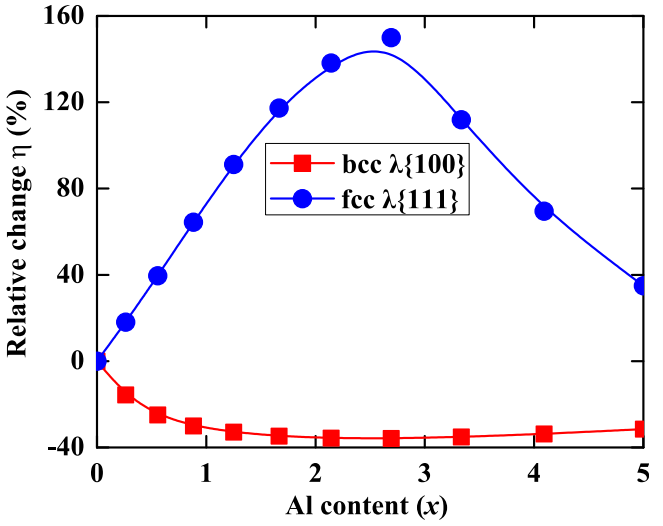

Fig. 5. Theoretical ratio between the cleavage stress and the resolved shear modulus associated with the slip system for paramagnetic bcc and fcc $Al_xCrMnFeCoNi$ as a function of Al content. (For interpretation of the references to colour in this figure legend, the reader is referred to the Web version of this article.)

corresponding B/G criterion. We conclude that the Pugh criterion is consistent with Cauchy pressure criterion when the elastic anisotropy is properly accounted for.

Wang et al. [94] proposed an alternative model to estimate the brittle/ductile behavior of alloys. It is based on the theoretical cleavage stress

$$\sigma_{cl.}\{lmn\} = \left(\frac{E_{lmn}\gamma_{lmn}}{d_{lmn}}\right)^{1/2}$$

where $\{lmn\}$ is the cleavage plane, E_{lmn}, γ_{lmn}, and d_{lmn} are the corresponding Young's modulus, surface energy, and interlayer distance, respectively. For bcc alloys, slip occurs primarily in the {110} plane along the <111> direction. The associated shear modulus can be expressed as $G\{110\}\langle 111\rangle = 3C_{44}C'/(C' + 2C_{44})$. Wang et al. [94] suggested that $\lambda\{110\}\equiv\sigma_{cl.}\{110\}/G\{110\}\langle 111\rangle$ as an indicator of the ductile/brittle behavior for bcc alloys. They proposed that larger λ corresponds to more ductile alloys. In fcc alloys, slip occurs in the {111} plane along the <112> direction. The associated resolved shear modulus can be expressed as $G\{111\}\langle 112\rangle = 3C_{44}(C_{11} - C_{12})/(4C_{44} + C_{11} - C_{12})$. Generalizing the Wang's model to fcc metals, we get $\lambda\{111\}\equiv\sigma_{cl.}\{111\}/G\{111\}\langle 112\rangle$. Since we do not possess the surface energies for the present HEAs, here we adopt as simple averaging scheme $\gamma_{HEAs} = \sum_n c_n\gamma_n$ to estimate the surface energy of $Al_xCrMnFeCoNi$, where c_n is the concentration of each alloying element n, γ_n is the experimental (extrapolated) surface energy of alloying element n. These are 2.345, 1.543, 2.417, 2.522, 2.380, 1.143 J/m^2 [99] for Cr, Mn, Fe, Co, Ni and Al, respectively. We use the so estimated γ_{HEAs} for both γ_{111} and γ_{100} and plot the relative change $\eta=(\lambda(x)-\lambda(0))/\lambda(0)$ as a function of Al in Fig. 5 as a function of x.

We find that $\eta(x)$ calculated for the fcc and bcc $Al_xCrMnFeCoNi$ alloys have similar trend as the Pugh ratio and Cauchy pressure in the whole concentration x. η for bcc slightly increased at high Al-region, compared to the almost unchanged Pugh ratio and Cauchy pressure, which might be due to the fact that the true surface energy γ_{100} for the bcc structure has a stronger drop at high Al concentration due to the low surface energy of Al. Based on the Wang's model, we conclude that the fcc $Al_xCrMnFeCoNi$ alloys are brittle (ductile) at low and high (intermediate) Al regions, while the bcc $Al_xCrMnFeCoNi$ alloys are ductile in the low-Al region and become more brittle with increasing Al addition.

Finally, below we offer a simple but plausible explanation for the negative Cauchy pressure of PM fcc CrMnFeCoNi alloy. The Cauchy pressure, defined as $CP\equiv C_{12}-C_{44}$, can alternatively be expressed as $CP\equiv B\text{-}C_{44}\text{-}2/3\,C'$. Since C' has a small positive value (for dynamically stable lattices), positive Cauchy pressure assumes that the bulk modulus is larger than C_{44}. According to the EMTO[b] (0 K, This work) results in Table 1, the bulk modulus is slightly lower than C_{44}, implying a significant negative CP. For comparison, we also calculated the lattice parameter and elastic constants of Mn-free PM fcc CrFeCoNi alloy using the same volume interval as for EMTO[b] (0 K, This work). The lattice constant, B, C_{44}, C' and CP of PM fcc CrFeCoNi are 3.526 Å, 202 GPa, 178 GPa, 47 GPa, −6 GPa, respectively. Although C_{44} and C' turn out to be similar for the two alloys in question, the Cauchy pressures differ by 27 GPa, which is mainly due to the difference in the bulk moduli. The question is then why the bulk modulus of PM fcc CrMnFeCoNi alloy is lower by 26 GPa than that of PM fcc CrFeCoNi.

We recall that for the same structure and volume, a smaller bulk modulus should be reflected by a lower cohesive energy [83]. The cohesive energy E_{coh} can be calculated from the bulk and atomic energies according to

$$E_{coh}^{HEA} = \sum_{i=1}^{n} c_i E_{atom}^{i} - E_{bulk}^{HEA}$$

where E_{atom}^{i} is the atomic energy of the ith component, and E_{bulk}^{HEA} is the equilibrium bulk energy of the HEA. Unfortunately, the atomic energies are hard to obtain from direct EMTO calculations. Instead, here we derive E_{atom}^{i} by combining the experimental cohesive energies [100] with the total energies of pure metals calculated for their ground state structures. The experimental cohesive energy of Cr, Mn, Fe, Co and Ni are 301, 215, 315, 323, 326 mRy/atom,

respectively. For the cohesive energy of PM fcc CrMnFeCoNi we obtain 283 mRy/atom, which is 21 mRy/atom smaller than the cohesive energy of PM fcc CrFeCoNi (304 mRy/atom). Furthermore, the cohesive energy of PM fcc CrMnFeCoNi is also lower than 296 mRy/atom obtained by averaging the cohesive energies of the pure Cr, Mn, Fe, Co and Ni metals. In other words, the formation enthalpy of fcc PM CrMnFeCoNi is positive. Hence the relative low cohesive energy of PM fcc CrMnFeCoNi is consistent with its low bulk modulus. This is also the reason why the equiatomic Mn addition decreases the Cauchy pressure of CrMnFeCoNi compared to that of CrFeCoNi.

5. Conclusions

Using the first-principles EMTO method, we have investigated the single-crystal and polycrystalline elastic parameters, and single-crystal Young's moduli of paramagnetic bcc and fcc $Al_xCrMnFeCoNi$ ($0 \leq x \leq 5$) high-entropy alloys. In spite of the fact that the calculated lattice constants for both phases increase nearly linearly with increasing Al content, the predicted elastic parameters and Zener anisotropy possess very complex composition dependences. For both fcc and bcc structures, the largest (smallest) value of single-crystal Young's modulus always appears along the <111> (<100>) direction.

We have shown that equiatomic Mn addition to CrFeCoNi decreases the cohesive energy and thus its bulk modulus, which results in a sizable negative Cauchy pressure for PM fcc CrMnFeCoNi. The Cauchy pressure and Pugh ratio indicate that the bcc $Al_xCrMnFeCoNi$ alloys become more brittle with increasing Al content. On the other hand, the fcc $Al_xCrMnFeCoNi$ alloys are predicted to be brittle at low and high Al region and ductile at intermediate Al region. Compared to previous works on Mn-free alloys, we found that equiatomic Mn makes the $Al_xCrMnFeCoNi$ system more brittle.

We find that the Cauchy and the original Pugh criteria for ductility are consistent when the Zener anisotropy A_Z is close to 1, but become inconsistent when A_Z is large. We show that the Zener anisotropy ratios of the $Al_xCrMnFeCoNi$ alloys are very large, which should be accounted for to remove the discrepancy between the two approaches. The Wang's model gives similar trends with those suggested by the modified Pugh and Cauchy criteria. Nevertheless, when considering the absolute values of the Cauchy pressures, most of the present HEAs are predicted to be brittle which contradicts the experimental observations. We invite experimentalists and theoreticians to further verify this interesting phenomenon and propose new revised ductility/brittleness versus metallic/covalent criterion for HEAs.

Acknowledgement

X. Sun acknowledges helpful discussions with W. Li, S. Huang, and S. Schönecker. The Fundamental Research Funds for the Central Universities, the National Key Research and Development Program of China (No.2016YFB0701302), the National Basic Research Program of China (No.2014CB644003), the Swedish Research Council (VR), the Swedish Foundation for Strategic Research (SSF), the Swedish Foundation for International Cooperation in Research and Higher Education (STINT), the Carl Tryggers Foundations, the Swedish Governmental Agency for Innovation Systems (VINNOVA), the China Scholarship Council, the Swedish Energy Agency and the Hungarian Scientific Research Fund (research project OTKA 109570) are acknowledged for financial support. Y. W. acknowledges the financial support of NSF under Grant DMR-1534826.

References

[1] J.W. Yeh, S.K. Chen, S.J. Lin, J.Y. Gan, T.S. Chin, T.T. Shun, C.H. Tsau, S.Y. Chang, Nanostructured high-entropy alloys with multiple principal elements: novel alloy design concepts and outcomes, Adv. Eng. Mater. 6 (5) (2004) 299–303.
[2] B. Cantor, I.T.H. Chang, P. Knight, A.J.B. Vincent, Microstructural development in equiatomic multicomponent alloys, Mater. Sci. Eng., A 375–377 (2004) 213–218.
[3] J.W. Yeh, S.K. Chen, J.Y. Gan, S.J. Lin, T.S. Chin, T.T. Shun, C.H. Tsau, S.Y. Chang, Formation of simple crystal structures in Cu-Co-Ni-Cr-Al-Fe-Ti-V alloys with multiprincipal metallic elements, Metall. Mater. Trans. A 35A (8) (2004) 2533–2536.
[4] J.W. Yeh, Y.L. Chen, S.J. Lin, S.K. Chen, High-entropy alloys - a new era of exploitation, Mater. Sci. Forum 560 (2007) 1–9.
[5] F. Otto, A. Dlouhy, C. Somsen, H. Bei, G. Eggeler, E.P. George, The influences of temperature and microstructure on the tensile properties of a CoCrFeMnNi high-entropy alloy, Acta Mater. 61 (15) (2013) 5743–5755.
[6] B. Gludovatz, A. Hohenwarter, D. Catoor, E.H. Chang, E.P. George, R.O. Ritchie, A fracture-resistant high-entropy alloy for cryogenic applications, Science 345 (6201) (2014) 1153–1158.
[7] S. Sohn, Y. Liu, J. Liu, P. Gong, S. Prades-Rodel, A. Blatter, B.E. Scanley, C.C. Broadbridge, J. Schroers, Noble metal high entropy alloys, Scr. Mater. 126 (2017) 29–32.
[8] O.N. Senkov, G.B. Wilks, D.B. Miracle, C.P. Chuang, P.K. Liaw, Refractory high-entropy alloys, Intermetallics 18 (9) (2010) 1758–1765.
[9] O.N. Senkov, G.B. Wilks, J.M. Scott, D.B. Miracle, Mechanical properties of $Nb_{25}Mo_{25}Ta_{25}W_{25}$ and $V_{20}Nb_{20}Mo_{20}Ta_{20}W_{20}$ refractory high entropy alloys, Intermetallics 19 (5) (2011) 698–706.
[10] S. Maiti, W. Steurer, Structural-disorder and its effect on mechanical properties in single-phase TaNbHfZr high-entropy alloy, Acta Mater. 106 (2016) 87–97.
[11] M.C. Gao, B. Zhang, S.M. Guo, J.W. Qiao, J.A. Hawk, High-entropy alloys in hexagonal close-packed structure, Metall. Mater. Trans. A 47 (7) (2016) 3322–3332.
[12] Y. Zhang, T.T. Zuo, Z. Tang, M.C. Gao, K.A. Dahmen, P.K. Liaw, Z.P. Lu, Microstructures and properties of high-entropy alloys, Prog. Mater. Sci. 61 (2014) 1–93.
[13] D.B. Miracle, J.D. Miller, O.N. Senkov, C. Woodward, M.D. Uchic, J. Tiley, Exploration and development of high entropy alloys for structural applications, Entropy 16 (1) (2014) 494–525.
[14] L.J. Santodonato, Y. Zhang, M. Feygenson, C.M. Parish, M.C. Gao, R.J.K. Weber, J.C. Neuefeind, Z. Tang, P.K. Liaw, Deviation from high-entropy configurations in the atomic distributions of a multi-principal-element alloy, Nat. Commun 6 (2015) 5964.
[15] P.F. Yu, L.J. Zhang, H. Cheng, H. Zhang, M.Z. Ma, Y.C. Li, G. Li, P.K. Liaw, R.P. Liu, The high-entropy alloys with high hardness and soft magnetic property prepared by mechanical alloying and high-pressure sintering, Intermetallics 70 (2016) 82–87.
[16] Z. Li, K.G. Pradeep, Y. Deng, D. Raabe, C.C. Tasan, Metastable high-entropy dual-phase alloys overcome the strength-ductility trade-off, Nature 534 (7606) (2016) 227–230.
[17] Y. Shi, B. Yang, P. Liaw, Corrosion-Resistant high-entropy alloys: a review, Metals 7 (2) (2017) 43.
[18] T. Zuo, M.C. Gao, L. Ouyang, X. Yang, Y. Cheng, R. Feng, S. Chen, P.K. Liaw, J.A. Hawk, Y. Zhang, Tailoring magnetic behavior of CoFeMnNiX (X = Al, Cr, Ga, and Sn) high entropy alloys by metal doping, Acta Mater. 130 (2017) 10–18.
[19] D.B. Miracle, O.N. Senkov, A critical review of high entropy alloys and related concepts, Acta Mater. 122 (2017) 448–511.
[20] S. Gorsse, D.B. Miracle, O.N. Senkov, Mapping the world of complex concentrated alloys, Acta Mater. 135 (2017) 177–187.
[21] M.C. Gao, J.-W. Yeh, P.K. Liaw, Y. Zhang, High-entropy Alloys: Fundamentals and Applications, Springer, 2016.
[22] F. Zhang, Y. Wu, H. Lou, Z. Zeng, V.B. Prakapenka, E. Greenberg, Y. Ren, J. Yan, J.S. Okasinski, X. Liu, Y. Liu, Q. Zeng, Z. Lu, Polymorphism in a high-entropy alloy, Nat. Commun 8 (2017) 15687.
[23] N.L. Okamoto, S. Fujimoto, Y. Kambara, M. Kawamura, Z.M.T. Chen, H. Matsunoshita, K. Tanaka, H. Inui, E.P. George, Size effect, critical resolved shear stress, stacking fault energy, and solid solution strengthening in the CrMnFeCoNi high-entropy alloy, Sci. Rep 6 (2016) 35863.
[24] A. Gali, E.P. George, Tensile properties of high- and medium-entropy alloys, Intermetallics 39 (2013) 74–78.
[25] F. Otto, Y. Yang, H. Bei, E.P. George, Relative effects of enthalpy and entropy on the phase stability of equiatomic high-entropy alloys, Acta Mater. 61 (7) (2013) 2628–2638.
[26] A.J. Zaddach, C. Niu, C.C. Koch, D.L. Irving, Mechanical properties and stacking fault energies of NiFeCrCoMn high-entropy alloy, JOM 65 (12) (2013) 1780–1789.
[27] K. Tanaka, T. Teramoto, R. Ito, Monocrystalline elastic constants of fcc-CrMnFeCoNi high entropy alloy, MRS Adv 2 (27) (2017) 1429–1434.
[28] A. Haglund, M. Koehler, D. Catoor, E.P. George, V. Keppens, Polycrystalline elastic moduli of a high-entropy alloy at cryogenic temperatures, Intermetallics 58 (2015) 62–64.
[29] G. Laplanche, P. Gadaud, O. Horst, F. Otto, G. Eggeler, E.P. George,

Temperature dependencies of the elastic moduli and thermal expansion coefficient of an equiatomic, single-phase CoCrFeMnNi high-entropy alloy, J. Alloy. Comp. 623 (2015) 348–353.
[30] F. Otto, A. Dlouhý, K.G. Pradeep, M. Kuběnová, D. Raabe, G. Eggeler, E.P. George, Decomposition of the single-phase high-entropy alloy CrMnFeCoNi after prolonged anneals at intermediate temperatures, Acta Mater. 112 (2016) 40–52.
[31] N.L. Okamoto, K. Yuge, K. Tanaka, H. Inui, E.P. George, Atomic displacement in the CrMnFeCoNi high-entropy alloy - a scaling factor to predict solid solution strengthening, AIP Adv 6 (12) (2016), 125008.
[32] L.R. Owen, E.J. Pickering, H.Y. Playford, H.J. Stone, M.G. Tucker, N.G. Jones, An assessment of the lattice strain in the CrMnFeCoNi high-entropy alloy, Acta Mater. 122 (2017) 11–18.
[33] D.-H. Lee, M.-Y. Seok, Y. Zhao, I.-C. Choi, J. He, Z. Lu, J.-Y. Suh, U. Ramamurty, M. Kawasaki, T.G. Langdon, J.-i. Jang, Spherical nanoindentation creep behavior of nanocrystalline and coarse-grained CoCrFeMnNi high-entropy alloys, Acta Mater. 109 (2016) 314–322.
[34] B. Gludovatz, E.P. George, R.O. Ritchie, Processing, microstructure and mechanical properties of the CrMnFeCoNi high-entropy alloy, JOM 67 (10) (2015) 2262–2270.
[35] A.J. Zaddach, R.O. Scattergood, C.C. Koch, Tensile properties of low-stacking fault energy high-entropy alloys, Mater. Sci. Eng., A 636 (2015) 373–378.
[36] D. Ma, B. Grabowski, F. Körmann, J. Neugebauer, D. Raabe, Ab initio thermodynamics of the CoCrFeMnNi high entropy alloy: importance of entropy contributions beyond the configurational one, Acta Mater. 100 (2015) 90–97.
[37] S. Huang, W. Li, S. Lu, F. Tian, J. Shen, E. Holmström, L. Vitos, Temperature dependent stacking fault energy of FeCrCoNiMn high entropy alloy, Scr. Mater. 108 (2015) 44–47.
[38] X. Sun, H. Zhang, S. Lu, X. Ding, Y. Wang, L. Vitos, Phase selection rule for Al-doped CrMnFeCoNi high-entropy alloys from first-principles, Acta Mater. 140 (2017) 366–374.
[39] L.-Y. Tian, G. Wang, J.S. Harris, D.L. Irving, J. Zhao, L. Vitos, Alloying effect on the elastic properties of refractory high-entropy alloys, Mater. Des 114 (2017) 243–252.
[40] J.Y. He, W.H. Liu, H. Wang, Y. Wu, X.J. Liu, T.G. Nieh, Z.P. Lu, Effects of Al addition on structural evolution and tensile properties of the FeCoNiCrMn high-entropy alloy system, Acta Mater. 62 (2014) 105–113.
[41] C.J. Tong, Y.L. Chen, S.K. Chen, J.W. Yeh, T.T. Shun, C.H. Tsau, S.J. Lin, S.Y. Chang, Microstructure characterization of Al_xCoCrCuFeNi high-entropy alloy system with multiprincipal elements, Metall. Mater. Trans. A 36A (4) (2005) 881–893.
[42] K.B. Zhang, Z.Y. Fu, J.Y. Zhang, W.M. Wang, H. Wang, Y.C. Wang, Q.J. Zhang, J. Shi, Microstructure and mechanical properties of CoCrFeNiTiAl_x high-entropy alloys, Mater. Sci. Eng., A 508 (1–2) (2009) 214–219.
[43] W.R. Wang, W.L. Wang, S.C. Wang, Y.C. Tsai, C.H. Lai, J.W. Yeh, Effects of Al addition on the microstructure and mechanical property of Al_xCoCrFeNi high-entropy alloys, Intermetallics 26 (2012) 44–51.
[44] T. Yang, S. Xia, S. Liu, C. Wang, S. Liu, Y. Zhang, J. Xue, S. Yan, Y. Wang, Effects of Al addition on microstructure and mechanical properties of Al_xCoCrFeNi High-entropy alloy, Mater. Sci. Eng., A 648 (2015) 15–22.
[45] C.-M. Lin, C.-C. Juan, C.-H. Chang, C.-W. Tsai, J.-W. Yeh, Effect of Al addition on mechanical properties and microstructure of refractory Al_xHfNbTaTiZr alloys, J. Alloy. Comp. 624 (2015) 100–107.
[46] C.-Y. Hsu, C.-C. Juan, T.-S. Sheu, S.-K. Chen, J.-W. Yeh, Effect of aluminum content on microstructure and mechanical properties of Al_xCoCrFe$Mo_{0.5}$Ni high-entropy alloys, JOM 65 (12) (2013) 1840–1847.
[47] C.J. Tong, M.R. Chen, S.K. Chen, J.W. Yeh, T.T. Shun, S.J. Lin, S.Y. Chang, Mechanical performance of the Al_xCoCrCuFeNi high-entropy alloy system with multiprincipal elements, Metall. Mater. Trans. A 36A (5) (2005) 1263–1271.
[48] Y.F. Kao, T.J. Chen, S.K. Chen, J.W. Yeh, Microstructure and mechanical property of as-cast, -homogenized, and -deformed Al_xCoCrFeNi ($0 \le x \le 2$) high-entropy alloys, J. Alloy. Comp. 488 (1) (2009) 57–64.
[49] H.P. Chou, Y.S. Chang, S.K. Chen, J.W. Yeh, Microstructure, thermophysical and electrical properties in Al_xCoCrFeNi ($0 \le x \le 2$) high-entropy alloys, Mater. Sci. Eng., B 163 (3) (2009) 184–189.
[50] M. Ogura, T. Fukushima, R. Zeller, P.H. Dederichs, Structure of the high-entropy alloy Al_xCrFeCoNi: fcc versus bcc, J. Alloy. Comp. 715 (2017) 454–459.
[51] L. Vitos, Total-energy method based on the exact muffin-tin orbitals theory, Phys. Rev. B 64 (1) (2001), 014107.
[52] J.P. Perdew, K. Burke, M. Ernzerhof, Generalized gradient approximation made simple, Phys. Rev. Lett. 77 (18) (1996) 3865–3868.
[53] P. Soven, Coherent-potential model of substitutional disordered alloys, Phys. Rev. 156 (3) (1967) 809–813.
[54] B.L. Gyorffy, Coherent-potential approximation for a nonoverlapping-muffin-tin-potential model of random substitutional alloys, Phys. Rev. B 5 (6) (1972) 2382–2384.
[55] L. Vitos, I.A. Abrikosov, B. Johansson, Anisotropic lattice distortions in random alloys from first-principles theory, Phys. Rev. Lett. 87 (15) (2001), 156401.
[56] L. Vitos, The EMTO method and applications, in: Computational Quantum Mechanicals for Materials Engineers, Springer-Verlag, London, 2007.
[57] P.A. Korzhavyi, A.V. Ruban, I.A. Abrikosov, H.L. Skriver, Madelung energy for random metallic alloys in the coherent potential approximation, Phys. Rev. B 51 (9) (1995) 5773–5780.
[58] H.L. Zhang, B. Johansson, L. Vitos, Ab initio calculations of elastic properties of bcc Fe-Mg and Fe-Cr random alloys, Phys. Rev. B 79 (22) (2009), 224201.
[59] H.L. Zhang, M.P.J. Punkkinen, B. Johansson, S. Hertzman, L. Vitos, Single-crystal elastic constants of ferromagnetic bcc Fe-based random alloys from first-principles theory, Phys. Rev. B 81 (18) (2010), 184105.
[60] H.L. Zhang, N. Al-Zoubi, B. Johansson, L. Vitos, Alloying effects on the elastic parameters of ferromagnetic and paramagnetic Fe from first-principles theory, J. Appl. Phys. 110 (7) (2011), 073707.
[61] H.L. Zhang, B. Johansson, R. Ahuja, L. Vitos, First-principles study of solid-solution hardening in steel alloys, Comput. Mater. Sci. 55 (0) (2012) 269–272.
[62] H.L. Zhang, M.P.J. Punkkinen, B. Johansson, L. Vitos, Elastic parameters of paramagnetic iron-based alloys from first-principles calculations, Phys. Rev. B 85 (5) (2012), 054107.
[63] H.L. Zhang, G. Wang, M.P.J. Punkkinen, S. Hertzman, B. Johansson, L. Vitos, Elastic anomalies in Fe-Cr alloys, J. Phys. Condens. Matter 25 (19) (2013), 195501.
[64] H.L. Zhang, X. Li, S. Schönecker, H. Jesperson, B. Johansson, L. Vitos, Anomalous elastic hardening in Fe-Co alloys at high temperature, Phys. Rev. B 89 (18) (2014), 184107.
[65] H. Zhang, S. Lu, M. Zhou, M.P.J. Punkkinen, B. Johansson, L. Vitos, Ab initio determination of the elastic properties of ferromagnetic body-centered cubic Fe-Mn-Al alloys, J. Appl. Phys. 118 (10) (2015), 103904.
[66] F.Y. Tian, L.K. Varga, N.X. Chen, L. Delczeg, L. Vitos, Ab initio investigation of high-entropy alloys of 3d elements, Phys. Rev. B 87 (7) (2013), 075144.
[67] F.Y. Tian, L. Delczeg, N.X. Chen, L.K. Varga, J. Shen, L. Vitos, Structural stability of NiCoFeCrAl_x high-entropy alloy from ab initio theory, Phys. Rev. B 88 (8) (2013), 085128.
[68] F. Tian, L.K. Varga, N. Chen, J. Shen, L. Vitos, Ab initio design of elastically isotropic TiZrNbMoV_x high-entropy alloys, J. Alloy. Comp. 599 (2014) 19–25.
[69] S. Huang, W. Li, X. Li, S. Schönecker, L. Bergqvist, E. Holmström, L.K. Varga, L. Vitos, Mechanism of magnetic transition in FeCrCoNi-based high entropy alloys, Mater. Des 103 (2016) 71–74.
[70] B.L. Gyorffy, A.J. Pindor, J. Staunton, G.M. Stocks, H. Winter, A first-principles theory of ferromagnetic phase transitions in metals, J. Phys. F Met. Phys. 15 (6) (1985) 1337.
[71] G.A. Alers, J.R. Neighbours, Crystal stability and elastic constants, J. Appl. Phys. 28 (12) (1957), 1514–1514.
[72] V.L. Moruzzi, J.F. Janak, K. Schwarz, Calculated thermal properties of metals, Phys. Rev. B 37 (2) (1988) 790–799.
[73] Z. Dong, W. Li, D. Chen, S. Schönecker, M. Long, L. Vitos, Longitudinal spin fluctuation contribution to thermal lattice expansion of paramagnetic Fe, Phys. Rev. B 95 (5) (2017), 054426.
[74] Z. Dong, S. Schönecker, D. Chen, W. Li, M. Long, L. Vitos, Elastic properties of paramagnetic austenitic steel at finite temperature: longitudinal spin fluctuations in multicomponent alloys, Phys. Rev. B 96 (17) (2017), 174415.
[75] Z. Dong, S. Schönecker, W. Li, D. Chen, L. Vitos, Thermal spin Fluctuations in CoCrFeMnNi High Entropy alloy, (unpublished).
[76] R. Hill, The elastic behaviour of a crystalline aggregate, Proc. Phys. Soc. 65 (5) (1952) 349.
[77] F. Tian, L.K. Varga, J. Shen, L. Vitos, Calculating elastic constants in high-entropy alloys using the coherent potential approximation: current issues and errors, Comput. Mater. Sci. 111 (2016) 350–358.
[78] Y. Wu, W.H. Liu, X.L. Wang, D. Ma, A.D. Stoica, T.G. Nieh, Z.B. He, Z.P. Lu, In-situ neutron diffraction study of deformation behavior of a multi-component high-entropy alloy, Appl. Phys. Lett. 104 (5) (2014), 051910.
[79] D.G. Pettifor, Theoretical predictions of structure and related properties of intermetallics, Mater. Sci. Technol 8 (4) (1992) 345–349.
[80] S.L. Shang, A. Saengdeejing, Z.G. Mei, D.E. Kim, H. Zhang, S. Ganeshan, Y. Wang, Z.K. Liu, First-principles calculations of pure elements: equations of state and elastic stiffness constants, Comput. Mater. Sci. 48 (4) (2010) 813–826.
[81] H. Zhang, B. Johansson, L. Vitos, Density-functional study of paramagnetic iron, Phys. Rev. B 84 (14) (2011), 140411(R).
[82] J. Zarestky, C. Stassis, Lattice dynamics of γ-Fe, Phys. Rev. B 35 (9) (1987) 4500–4502.
[83] G. Grimvall, Thermophysical Properties of Materials, Elsevier, New York/Amsterdam, 1999.
[84] H.M. Ledbetter, Elastic properties of zinc: a compilation and a review, J. Phys. Chem. Ref. Data 6 (4) (1977) 1181–1203.
[85] K.M. Knowles, P.R. Howie, The directional dependence of elastic stiffness and compliance shear coefficients and shear moduli in cubic materials, J. Elasticity 120 (1) (2015) 87–108.
[86] G. Grimvall, Polymorphism of metals. Iii. Theory of the temperature-pressure phase diagram of iron, Phys. Scripta 13 (1) (1976) 59.
[87] Y. Wang, M. Yan, Q. Zhu, W.Y. Wang, Y. Wu, X. Hui, R. Otis, S.-L. Shang, Z.-K. Liu, L.-Q. Chen, Computation of entropies and phase equilibria in refractory V-Nb-Mo-Ta-W high-entropy alloys, Acta Mater. 143 (2018) 88–101.
[88] Y. Wang, Z.K. Liu, L.Q. Chen, Thermodynamic properties of Al, Ni, NiAl, and Ni_3Al from first-principles calculations, Acta Mater. 52 (9) (2004) 2665–2671.
[89] F. Körmann, Y. Ikeda, B. Grabowski, M.H.F. Sluiter, Phonon broadening in high entropy alloys, NPJ Comput. Mater. 3 (1) (2017).

[90] Y. Ikeda, F. Körmann, B. Dutta, A. Carreras, A. Seko, J. Neugebauer, I. Tanaka, Temperature-dependent phonon spectra of magnetic random solid solutions, NPJ Comput. Mater. 4 (1) (2018).
[91] S.F. Pugh, XCII, Relations between the elastic moduli and the plastic properties of polycrystalline pure metals, The London, Edinburgh, and Dublin Philosophical Magazine and Journal of Science 45 (1954) 823–843.
[92] W. Feng, Y. Qi, S. Wang, Effects of short-range order on the magnetic and mechanical properties of FeCoNi(AlSi)$_x$ high entropy alloys, Metals 7 (11) (2017) 482.
[93] S. Cui, D. Wei, H. Hu, W. Feng, Z. Gong, First-principles study of the structural and elastic properties of Cr_2AlX (X=N, C) compounds, J. Solid State Chem. 191 (2012) 147–152.
[94] G. Wang, S. Schönecker, S. Hertzman, Q.-M. Hu, B. Johansson, S.K. Kwon, L. Vitos, Ab initio prediction of the mechanical properties of alloys: the case of Ni/Mn-doped ferromagnetic Fe, Phys. Rev. B 91 (22) (2015), 224203.
[95] X. Wang, Y.-T. Zhang, P.-C. Liu, J. Yan, W. Mo, P.-C. Zhang, X.-Q. Chen, Ductile-to-brittle transition and materials' resistance to amorphization by irradiation damage, RSC Adv 6 (50) (2016) 44561–44568.
[96] Q. Meng, S. Guo, X. Ren, H. Xu, X. Zhao, Possible contribution of low shear modulus C_{44} to the low Young's modulus of Ti-36Nb-5Zr alloy, Appl. Phys. Lett. 105 (13) (2014), 131907.
[97] L. Romaner, C. Ambrosch-Draxl, R. Pippan, Effect of rhenium on the dislocation core structure in tungsten, Phys. Rev. Lett. 104 (19) (2010) 195503.
[98] G. Wang, Q.-M. Hu, K. Kokko, B. Johansson, L. Vitos, Ab initio investigation of the elastic properties of Ni_3Fe, Phys. Rev. B 88 (17) (2013), 174205.
[99] L. Vitos, A.V. Ruban, H.L. Skriver, J. Kollár, The surface energy of metals, Surf. Sci. 411 (1) (1998) 186–202.
[100] C. Kittel, Introduction to Solid State Physics, eighth ed., Wiley, 2005.